Scattering Patterns of Self-Assembled Cubic Phases. 2. Analysis of the Experimental Spectra

Piotr Garstecki and Robert Hołyst*

Institute of Physical Chemistry, Polish Academy of Sciences, Department III, Kasprzaka 44/52, 01-224 Warsaw, Poland

Received August 15, 2001

The method presented in the preceding article is applied in this paper to the analysis of X-ray spectra of cubic phases formed in the following systems: 1,2-dilauoryl-*sn*-glycero-3-phosphoethanolamine, 1,2-dielaidoyl-*sn*-glycero-3-phosphoethanolamine, 1,2-dioleoyl-*sn*-glycero-3-phosphocholine, and didodecyldimethylammonium bromide lipids in water; glycerolmonooleate amphiphilic molecules with Polaxamer P407 in water; $R_6^F\Sigma EO_2$ fluorinated surfactants in aqueous solutions and polimerized system formed in the cetyltrimethylammonium chloride with tetraethyl orthosilicate additives. We show that our analysis allows determination of the width of the layer decorating the periodic surface in the cubic phase, the composition of the cubic phase in the system with excess water, the type of the cubic phase (direct or inverse), surface area per head of the amphiphilic molecule, the volume fractions of the coexisting cubic phases, the epitaxial relations between the coexisting phases, and the kinetic pathways in the phase transitions between ordered phases.

1. Introduction

In the preceding paper[1] we have presented data for the scattering intensities of the strongest reflections for seven (P, D, G, I-WP, C(P), C(D), F-RD) triply periodic minimal surface (TPMS) based cubic phases. In this article we want to show applications of the theoretical model for the scattering intensities to the analysis of the experimental spectra.

We have applied our method to several systems out of which nine are presented in this work. We have classified the systems into five groups. The first one includes the 1,2-dilauoryl-*sn*-glycero-3-phosphoethanolamine (DLPE), 1,2-dielaidoyl-*sn*-glycero-3-phosphoethanolamine (DEPE), and 1,2-dioleoyl-*sn*-glycero-3-phosphocholine (DOPE) lipid aqueous dispersions. These lipid molecules are a part of a large class of lipids containing the -phosphatocholine part. They are commonly used to explore the phase diagrams of amphiphilic mixtures. Another example of a very popular amphiphilic molecule is the monoglyceride (GMO). We present a study of two systems with GMO. The third compound that has attracted a lot of experimental attention is the didodecyldimethylammonium bromide (DDAB) lipid (analysis of one such system is presented here). We decided to include also a fit for the scattering pattern of a polimerized structure formed in CTAS with TEOS additives. This study is motivated by a growing scientific and technological interest in microporous and mesoporous materials formed on surfactant templates by the polymerization of silicates (like tetraethyl orthosilicate (TEOS)). Finally we study a scattering pattern for a cubic phase of the $R_6^F\Sigma EO_2$ fluorinated surfactant in water.

As it will be discussed in detail in the third section, the analysis yielded interesting insight into the explored structures. In two cases we have discovered the phase coexistence between cubic-lamellar and cubic-hexagonal phases (see sections 3.1.2 and 3.3) and established the epitaxial relations between them. The method has also been applied to a system of a known phase coexistence of a P and D structures observed in a fast cooling (0.5 deg/min) temperature scan experiment (section 3.1.4). In this example we extract from the full X-ray spectrum the part of it which corresponds to the third unknown phase (probably metastable) forming during the phase transition. In principle such analyses shed light on the kinetics of phase transitions between ordered phases.

Fitting the scattering pattern provides not only the TPMS on which the cubic phase is based but also its macro- and mesoscale characteristics, such as layer width (decorating TPMS), volume fractions of the coexisting phases, area per head of a surfactant molecule, and composition of the cubic phases in the presence of the excess water in the system. Scattering patterns give also, in many cases, a clear distinction between a direct or an inverse structure (see preceding paper[1]). This in turn, together with the layer width L, can be used to study the elasticity constants of a surfactant layer, preferred curvatures, and conformations of the hydrocarbon chains inside the layers.

The second section contains a step-by-step description of the method. The results of its application are inclosed in the third section.

2. The Method

In this section we want to present a detailed step-by-step approach toward analysis of the experimental scattering spectrum. To compare measured intensities with the modeled ones, we have to take into account the corrections due to the experimental setup. The first one is the Lorentz-polarization (LP) factor. Its form depends on the type of detector used to measure the scattering intensities. For a powder sample and a one-dimensional detector, the LP reads

$$\mathrm{LP}^{1\mathrm{D}}(\theta_{hkl}) = \frac{1}{2}\left(\frac{1+\cos^2 2\theta_{hkl}}{\sin 2\theta_{hkl}}\right) \qquad (1)$$

where θ_{hkl} is the scattering angle, related to the scattering vector $\mathbf{q} = (2\pi/a)[h,k,l]$ by the formula

* Corresponding author. E-mail: holyst@saka.ichf.edu.pl, http://www.ichf.edu.pl/Dep3.html.

(1) Garstecki, P.; Hołst, R. *Langmuir* **2002**, *18*, 2519−2528.

10.1021/la011299h CCC: $22.00
Published on Web 03/09/2002

$$\sin\theta_{hkl} = \lambda q/4\pi \tag{2}$$

Here λ is the wavelength of the radiation and a is the lattice parameter of the unit cell (linear size). For a two-dimensional detector, the LP has a slightly different form

$$\mathrm{LP}^{2D}(\theta_{hkl}) = \frac{1}{4}\left(\frac{1+\cos^2 2\theta_{hkl}}{\sin^2\theta_{hkl}\cos\theta_{hkl}}\right) \tag{3}$$

In most of the cases analyzed in this work, we have assumed that the data presented in the experimental reports have been LP corrected. In some cases we have not used the LP factor, because of private communication with the authors or the quality of the fits. We have also chosen to neglect other corrections such as an absorption coefficient, the multiple scattering effect, etc. Thus, the experimental intensities which will be compared with the modeled ones are obtained by dividing the raw experimental data by a correct LP factor and subtracting the background intensity

$$I_{hkl}^{(\mathrm{exp})} = \frac{I_{hkl}^{(\mathrm{raw})}}{\mathrm{LP}(\theta_{hkl})} - I^{(\mathrm{bg})}(q_{hkl}) \tag{4}$$

When the experimental resolution is small, the background scattering can be easily extracted. In most of the cases presented in this paper, we have established the background intensity on the basis of experimental data, where the Bragg peaks usually sit on a well-defined broad scattering pattern. In two cases the background intensity resembled the scattering pattern from the microemulsion with a characteristic broad maximum. In these cases it was fitted with the scattering intensity for a microemulsion system given by[2]

$$I^{(\mathrm{bg})}(q) = \frac{I_0}{\left(1-\frac{I_0}{I_{\max}}\right)\left(\frac{q^2}{{q_{\max}}^2}-1\right)^2 + \frac{I_0}{I_{\max}}} \tag{5}$$

where I_0 is the intensity for $q = 0$ and $q_{\max}$ is the scattering vector length for which the intensity attains maximum, $I_{\max}$.

When the raw experimental intensities are corrected according to the details of the experimental setup and the background intensity is subtracted, one can proceed with fitting the modeled intensities. The first step is to determine the peak spacing and the cubic cell parameter a. If more than one ascription of the hkl Miller indices is reasonable, all of the possibilities are checked via the following fitting procedure and the best fit is chosen.

The model amplitudes for the TPS-based cubic phases have been described in detail in the preceding article.[1] Here, to fit the data we will use the simplified model which assumes a flat contrast density profile $\rho(\xi) = \rho_0$ for $|\xi| \le L/2$ and $\rho(\xi) = 0$ for $|\xi| > L/2$, where L is the width of the layer decorating the base minimal surface and ξ is a coordinate along the direction normal to the surface. Also the fluctuations of the layer will be neglected. Within this approximation the model scattering amplitude is

$$A(\mathbf{q}, L) = F^{\mathrm{S}}\frac{2\rho_0}{\alpha_{hkl}q}\sin\left(\alpha_{hkl}q\frac{L}{2}\right) \tag{6}$$

where $q = (2\pi/a)(h^2 + k^2 + l^2)^{1/2}$ is the length of the scattering wave vector. Since in comparison with experiment only the relative amplitudes matter, to simplify this expression we can divide it by the factor $2a^3\rho_0$, which is constant for all hkl reflections. Finally the model scattering intensities are given by the equation

$$I_{hkl}^{(\mathrm{mod})}(L) = \mathscr{M}_{hkl}\left[F_{hkl}^{\mathrm{S}*}\frac{\sin(\alpha_{hkl}\pi(h^2+k^2+l^2)^{1/2}L^*)}{\alpha_{hkl}2\pi(h^2+k^2+l^2)^{1/2}}\right] \tag{7}$$

where $L^* = L/a$ is a dimensionless layer width expressed in terms of the lattice constant a and all of the constants, the dimensionless structure factor $F^{\mathrm{S}*} = F^{\mathrm{S}}/a^2$, multiplicity factor $\mathscr{M}_{hkl}$, and the correction parameters α_{hkl}, are explicitly given in Tables 2−8 of ref 1 for the P, D, G, C(D), C(P), F-RD, and I-WP based cubic phases.

Since the scattering intensity is measured on an arbitrary scale, only the relative intensities of subsequent peaks can be determined. Thus, to fit the experimental data, the model intensities have to be multiplied by a normalization constant Z, which is chosen in such a way as to set the model intensity of one reference HKL peak to be exactly equal the experimental intensity.

$$Z = I_{\mathrm{HKL}}^{(\mathrm{exp})}/I_{\mathrm{HKL}}^{(\mathrm{mod})} \tag{8}$$

In all of the examples presented below, we have chosen the first nonzero reflection as the reference peak. Then we checked whether any of the modeled structures satisfies the following relation

$$I_{hkl}^{(\mathrm{exp})} \simeq ZI_{hkl}^{(\mathrm{mod})}(L^*)\ \forall\ hkl \tag{9}$$

for any layer width L. The object to find the actual width of the layer decorating the minimal surface can be achieved by simply comparing the set of experimental intensities $I_{hkl}^{(\mathrm{exp})}$ with the modeled $I_{hkl}^{(\mathrm{mod})}(L^*)$ ones for various layer widths. In practice it is numerically easier to look for the model scattering patterns best resembling the experimental ones when they are both expressed as continuous curves rather then a set of distinct values. The experimental and numerical intensity curves $I^{(\mathrm{exp/mod})}(q)$ have been reconstructed by a convolution of the set of $I_{hkl}^{(\mathrm{exp/mod})}$ values with the Gaussian resolution function $R(q) = \exp(-q^2/2\sigma_r^2)/(\sigma_r(2\pi)^{1/2})$. The σ_r parameter is directly related to the half-widths $\delta I_{1/2}$ of the experimental peaks $\sigma_r \approx (1/2.3)\delta I_{1/2}$

$$I^{(\mathrm{exp/mod})}(q) = \frac{1}{\sigma_r(2\pi)^{1/2}}\sum_{hkl}\exp\left[\frac{-(q_{hkl}-q)^2}{2{\sigma_r}^2}\right]I_{hkl}^{(\mathrm{exp/mod})} \tag{10}$$

Thus instead of comparing the h, k, l peak intensities, we have performed a minimization of the following integral

$$\Delta(L) = \int_0^\infty \mathrm{d}q\left(I^{(\mathrm{exp})}(q) - ZI^{(\mathrm{mod})}(q, L^*)\right)^2 \rightarrow \text{minimum} \tag{11}$$

with the variation parameter being the dimensionless layer width L^*. Then the optimal layer width $L = aL^*$ (for which $\Delta(L^*)$ is minimal) has been assumed to be the real width of the layer decorating the base minimal surface.

Having established the width of the layer, one can proceed with further analysis of the structure of the cubic phase. The following relation

(2) Teubner, M.; Strey, R. *J. Chem. Phys.* **1987**, *87*, 3195−3200.

$$\phi = s_0{}^*L^* + \frac{\pi}{6}\chi L^{*3} \tag{12}$$

yields the volume fraction ϕ of the layer. The dimensionless surface area $s_0{}^* = s_0/a^2$ of the base TPMS and its Euler characteristic χ are given in Table 1 of the preceding paper.[1]

To tell whether a direct or inverse structure has been formed, one can compare ϕ with the volume fractions of water (ϕ_w), surfactant (ϕ_s), and hydrocarbons (ϕ_h) in the system. A layer volume fraction ϕ comparable with the water volume fraction $\phi \approx \phi_w$ stands in favor of the direct phase, when the minimal surface is decorated with a water film. When ϕ is comparable with the joint volume fraction of surfactant and hydrocarbon, $\phi \approx \phi_s + \phi_h$, more likely the inverse phase has been formed with the minimal surface draped with the surfactant bilayer. Still this method has a serious weakness. In many systems the cubic phases coexist with an excess water phase. Thus the system's composition does not reflect the composition of the cubic phase itself. Therefore a more reliable analysis is needed. It is based on the estimation of the surface area per surfactant head a_s as follows. The layer decorating the minimal surface is confined between two parallel surfaces laying at a distance $L/2$ away from the base minimal surface. The surface area per unit cell of these two interfaces is given by

$$s_{||}(L) = 2s_0{}^*a^2 + \pi\chi L^2 \tag{13}$$

The parallel surfaces divide the volume into three regions: the layer and two disjoint continuous channels. In the case of the direct phase, the hydrocarbon and surfactant molecules occupy the two channels. Its volume per unit cell is equal to $V_{dir} = (1 - \phi)\, a^3$. When an inverse structure is formed, the amphiphilic and hydrophobic molecules reside within the layer of a volume per unit cell equal to $V_{inv} = \phi a^3$. Knowing the molecular weight of the surfactant M (g/mol), the densities of surfactant and hydrocarbon (ρ_s (g/cm^3) and ρ_h (g/cm^3), respectively), and the weight fractions of surfactant and hydrocarbon in the system (x_s and x_h), one can establish the number of surfactant molecules per cubic cell

$$N_{dir/inv}(L) = V_{dir/inv}\frac{N_A}{M}\left(\frac{\rho_s}{1 + \frac{x_h\rho_s}{x_s\rho_h}}\right) \times 10^{-24} \tag{14}$$

where $N_A = 6.023 \times 10^{23}$ is the Avogadro constant and the factor 10^{-24} comes from the ratio of the cubic centimeter to cubic angström (1 cm^3 = 10^{24} Å^3). Finally the area per surfactant head

$$a_{s\ dir/inv}(L) = s_{||}(L)N_{dir/inv}(L) \tag{15}$$

In this approach we assume that all of the hydrocarbons present in the system are confined within the surfactant bilayer or channel. In the case of a binary mixture, the term in parentheses in eq 14 simplifies to the surfactant density. The density of surfactant is in principle an unknown feature as it can vary from one ordered phase to another. Still, as shown in the examples below, the dependence of the surface area per surfactant head on the layer width is strong enough to settle with an approximated density. In most cases, the plot of $a_{s,dir}$ and $a_{s,inv}$ against the layer volume fraction enables unambiguous determination of the type of the structure.

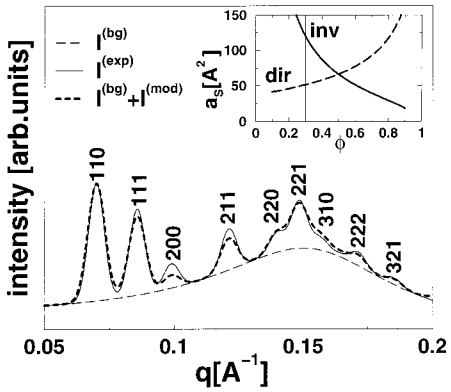

Figure 1. The fit of the experimental scattering pattern reported in ref 3. The solid line shows the experimental intensity curve reproduced using eq 10. The thin dashed line gives the background intensity fitted through eq 5. The thick solid line presents the theoretical fit for the D-based cubic phase of the layers volume fraction $\phi = 0.3$. The areas per lipid head for a direct and an inverse type of the D structure are drawn in the inset (dashed and solid lines respectively). For $\phi = 0.3$ the area per lipid is $a_{s,dir} \approx 50$ Å^2 for the direct phase and $a_{s,inv} \approx 120$ Å^2 for an inverse type. This indicates a D-based direct cubic phase of the water film volume fraction $\phi = 0.3$.

3. Analysis of the Experimental Spectra

3.1. The DLPE, DEPE, and DOPE Systems. The DEPE/Water System. 3.1.1. The DEPE/Water System.[3] The system is composed of 1,2-dielaidoyl-*sn*-glycero-3-phosphoethanolamine (DEPE) dispersion in an excess water phase. The diffraction pattern consists of nine Bragg reflections. Their spacing ($\sqrt{2}$, $\sqrt{3}$, $\sqrt{4}$, $\sqrt{6}$, $\sqrt{8}$, $\sqrt{9}$, $\sqrt{10}$, $\sqrt{12}$, $\sqrt{14}$) indicates a $Pn\bar{3}m$ symmetry (No. 224 in the International Crystallography Tables). The most commonly encountered structure of this symmetry is the double diamond D surface based phase. This assumption proved to be correct. Minimizing the integral eq 11 yielded the layer width $L = 0.162a$. This value correspond to the layer volume fraction $\phi = 0.3$. The experimental scattering pattern together with the model fit is shown in Figure 1. In addition we have been able to identify the background scattering intensity as the scattering from the microemulsion (eq 5 with parameters $I_0 = 0.174I_{110}$, $I_{max} = 0.714I_{110}$, and $q_{max} = 0.15$ Å^{-1}). This indicates that the cubic monocrystalline regions are separated by volumes filled with disordered bicontinuous phase.

The inset of Figure1 shows the area per surfactant head as a function of the layer volume fraction ϕ. The molecular weight of DOPE is $M_{DOPE} = 744$ (g/mol). In our calculations we have assumed its density to be equal to unity ($\rho_{DOPE} = 1$). For $\phi \approx 0.3$ the area per head is $a_{s,dir} \approx 50$ Å^2 or $a_{s,inv} \approx 120$ Å^2. The comparison of these two values strongly supports the direct phase (dir) with a water film decorating the minimal surface.

Since the system is prepared with excess water, it is important to note here that determining the layer width L and the structure type is a direct way of establishing the composition of the cubic phase.

3.1.2. The DLPE/α-Tocopherol/Water System.[4] The system under investigation contained a fully hydrated 1,2-dilauoryl-*sn*-glycero-3-phosphoethanolamine (DLPE) with an addition of 10 mol % α-tocopherol. The experimental scattering spectrum consisted of nine reflections $\sqrt{2}$, $\sqrt{3}$, $\sqrt{4}$, $\sqrt{6}$, $\sqrt{8}$, $\sqrt{9}$, $\sqrt{10}$, $\sqrt{12}$, $\sqrt{14}$ ($Pn\bar{3}m$ symmetry

(3) Keller, S. L.; Gruner, S. M.; Gawrisch, K. *Biochim. Biophys. Acta* **1996**, *1278*, 241−246.
(4) Wang, X.; Quinn, P. J. *Biophys. Chem.* **1999**, *80*, 93−101.

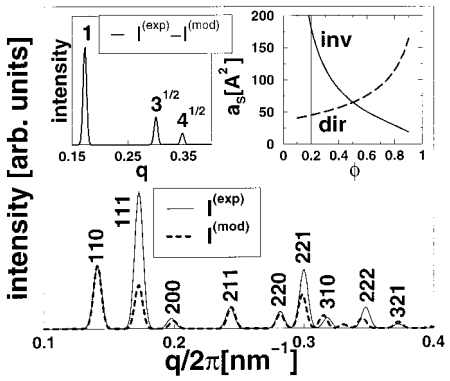

Figure 2. The fit of the experimental scattering pattern reported in ref 4. The solid line shows the experimental scattering curve, eq10, while the thick dashed line gives the theoretical fit for a D-based phase of the layer volume fraction $\phi = 0.2$. The very high intensity (in comparison with a fitted value) of the experimental 111, 221, and 222 peaks implies a coexistence with a hexagonal phase of a lattice parameter $a^{(\mathrm{hex})} = (2/3)a^{(\mathrm{D})}$. The intensity difference between the experimental and fitted curve is shown in the top left inset. The top right inset presents the areas per lipid head as a function of the layer volume fraction.

No. 224). The authors of ref 4 concluded that it is the double diamond D structure. It is partially right; Figure 2 shows the fit for the D structure ($\phi = 0.2$, $a_{\mathrm{s,dir}} \approx 45$ Å^2 and $a_{\mathrm{s,inv}} \approx 180$ Å^2 indicating a direct phase). Still the analysis of the peak positions only overlooks the phase coexistence with the hexagonal phase. All of the peaks are fitted very well besides the 111, 221, and 222 reflections spaced 1, $\sqrt{3}$, and $\sqrt{4}$, respectively. The inset in the upper left corner of Figure 2 shows the modeled intensity subtracted from the experimental data. The remaining peaks are characteristic of a hexagonal phase. A very similar phenomenon has been discovered in a 1,2-dioleoyl-*sn*-glycero-3-phosphocholine (DOPE) dispersion in water.[5] The reflections 10, 11, and 20 from the hexagonal phase were superimposed on the 111, 221, and 222 peaks originating from the double-diamond structure. What is particularly interesting is the ratio between the hexagonal and cubic cell parameters. The scattering vector length is related to the hexagonal lattice parameter by $q_{hk}{}^{(\mathrm{hex})} = (2\pi/a^{(\mathrm{hex})})(2/\sqrt{3})(h^2 + k^2 - hk)^{1/2}$ and for the cubic lattice $q_{hkl}{}^{(\mathrm{D})} = (2\pi/a^{(\mathrm{D})})(h^2 + k^2 + l^2)^{1/2}$. Since $q_{10}{}^{(\mathrm{hex})} = q_{111}{}^{(\mathrm{D})}$

$$q_{10}{}^{(\mathrm{hex})} = \frac{2\pi}{a^{(\mathrm{hex})}}\frac{2}{\sqrt{3}} = \frac{2\pi}{a^{(\mathrm{D})}}\sqrt{3} = q_{111}{}^{(\mathrm{D})} \qquad (16)$$

then $a^{(\mathrm{hex})} = (2/3)a^{(\mathrm{D})}$. The double-diamond structure consists of two separate continuous networks of rods connected four by four. If one looks at a projection of the node positions on a [111] plane perpendicular to the diagonal of the cubic cell, he would see a 2D hexagonal lattice with the lattice parameter $a^{(\mathrm{hex})} = (\sqrt{2}/\sqrt{3})a^{(\mathrm{D})}$ (Figure 3). It is significantly different from the one established from the scattering data. Thus the ratio $a^{(\mathrm{hex})} = (2/3)a^{(\mathrm{D})}$ seen in two different systems cannot be explained by a simple geometrical, epitaxial relationship. The relation between the lattice parameters could yield in principle interesting information on the elasticity constants of DLPE and DOPE monolayers.

3.1.3. The DOPE/Water System.[6] A 50 wt % DOPE−water dispersion was studied in a wide temperature range

(5) Angelova, A.; Ionov, R.; Koch, M. H. J.; Rapp, G. *Arch. Biochem. Biophys.* **2000**, *378*, 93−106.

(6) Erbes, J.; Czeslik, C.; Hahn, W.; Winter, R.; Rappolt, M.; Rapp, G. *Ber. Bunsen-Ges. Phys. Chem.* **1994**, *98*, 1287−1292.

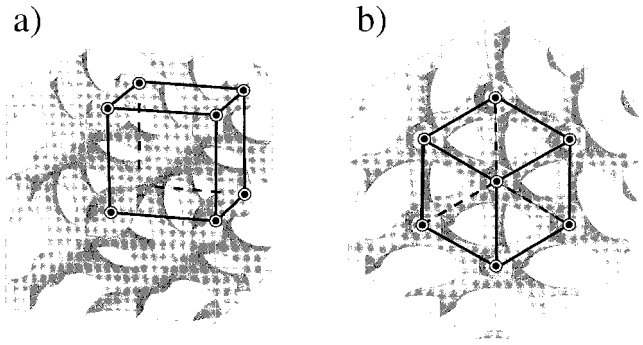

Figure 3. Visualization of the two disjoint channels forming the double-diamond periodic network. Part a shows the cubic cell of a lattice parameter $a^{(\mathrm{D})}$ used for the scattering spectrum evaluation. It is given by black lines with the vertexes marked with black in white circles. Part b shows the same network of channels seen along the diagonal of the cubic cell. The edges of the cubic cell form a two-dimensional hexagonal lattice of a parameter $a^{(\mathrm{hex})} = (\sqrt{2}/\sqrt{3})a^{(\mathrm{D})}$.

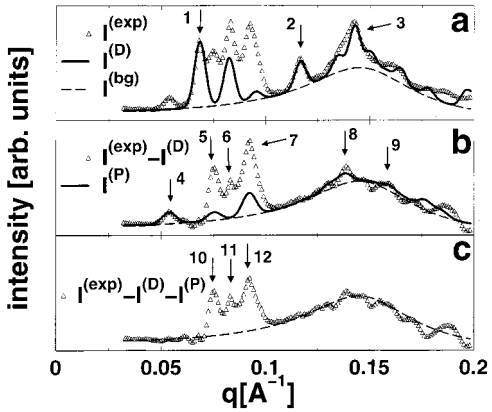

Figure 4. Analysis of a scattering spectrum recorded during a temperature scan of a GMO/P407/water system reported in ref 6. The experimental intensity curve is shown with open triangles in curve a. Also a fit for the background intensity (dashed line) and for the D-based phase of $\phi = 0.1$ (solid line) is shown. The arrows marked 1, 2, and 3 point to the 110 (1), 211 (2), and a group of the 220, 221, and 310 peaks (3) which are reconstructed very accurately. Then the intensity of the D-based phase is subtracted from the experimental curve. The remaining intensity curve is shown with open triangles in plot b. The solid line presents a theoretical intensity for a P-based phase ($\phi = 0.1$). After the P intensity is subtracted, only three peaks remain at spacing frequency $\sqrt{4}$, $\sqrt{5}$, and $\sqrt{6}$ marked with 10, 11, and 12, respectively. Further explanation is contained in section 3.1.4.

(4 °C < T < 80 °C). At high temperatures the hexagonal phase dominates the scattering pattern. However for temperatures below T = 30 °C several peaks of two coexisting cubic phases appear. The experimental scattering curve for T = 5 °C is presented in Figure 4a with open triangles. The pattern consists of the $\sqrt{2}$, $\sqrt{3}$, $\sqrt{6}$, and $\sqrt{9}$ reflections originating from the $Pn\bar{3}m$ symmetry with a 132 Å unit cell and $\sqrt{2}$, $\sqrt{4}$, and $\sqrt{6}$ peaks ($Im\bar{3}m$, 168 Å).

We begin the analysis with a fit of the background intensity. Figure 4a shows $I^{(\mathrm{bg})}$ (eq 5 with parameters $I_0 = 0.8I_1$, $I_{\max} = 4.7I_1$, and $q_{\max} = 0.145$ Å^{-1}, where I_1 corresponds to the intensity of the first peak located at 0.0529 Å). Next we assume that the $Pn\bar{3}m$ cubic phase is based on a double-diamond D TPMS. Minimization of the integral eq 11 yields a small volume fraction of the layer $\phi \in (0.1, 0.2)$. The fit is shown in Figure 4a with a solid line. The intensities of the 211 reflection (marked with an

index 2 on the figure) and the group of the 220, 221, and 310 peaks (marked with 3) are reconstructed very accurately, which supports the assumption on the structure type. The molecular weight of DOPE is $M_{DOPE} = 744$ (g/mol). Evaluating eq 15, we have obtained the following areas per surfactant head: $a_{s,dir} \in (40.3, 44.4)$ Å^2 and $a_{s,inv} \in (362.8, 177.7)$ Å^2. The values for the direct phase are similar to the ones computed for the systems described above. This fact, together with a good fit of the intensities, confirms a D direct structure. In the next step we subtract the modeled intensity for the D structure from the original experimental data. The remaining intensity contains four well-resolved peaks of the spacing $\sqrt{2}$:$\sqrt{4}$:~$\sqrt{5}$:$\sqrt{6}$ (in Figure 4b marked with the indices 4, 5, 6, and 7, respectively). If we assume that the $\sqrt{2}$:$\sqrt{4}$:$\sqrt{6}$ reflections originate from an $Im\bar{3}m$ cubic lattice, only the P-based phase could be fitted to these data. It means that the sequence should be 110, 200, and 211 reflections. Minimizing eq 11 gives a small volume fraction of the layer. This is also supported by the relatively large intensity of the 222, 321 reflections fitting the experimental peak marked by the index 8 on the figure and 400, 411 (mark 9). Moreover in the $\phi \in (0.1, 0.2)$ range of volume fractions, the area per surfactant head for the direct phase assumes reasonable values $a_{s,dir} \in (38.1, 42.2)$ Å^2. Thus if the assumption that the P structure has been formed is correct, most probably it would be a direct phase with a small volume fraction of the water film, the same as for the coexisting D structure.

After the intensity for the P structure is subtracted, the remaining intensity curve consists of three peaks $\sqrt{4}$:~$\sqrt{5}$:$\sqrt{6}$ (Figure 4c, marks 10, 11, and 12, respectively). A very similar pattern has been reported for a sodium dodecyl sulfate (SDS)/hydrocarbon/water system,[7] where it has been assigned to a $Pm\bar{3}n$ micellar cubic phase. The peaks could also be interpreted as evidence of some unidentified third phase separating the monocrystalline regions of D and P phases. As we have the data for only one temperature, it is impossible to risk any final judgment. A similar analysis of the scattering patterns during the whole temperature scan would probably give reliable answers. For example one could track the kinetics of the phase transition. Assuming that the D and P structure assignment is correct, one can extract approximate volume fractions of these phases. Namely, amplitude of the 000 reflection is proportional to the volume occupied by the layer decorating the minimal surface (see eq 6 in ref 1)

$$I_{000}(L) \propto [\phi(L)V]^2 \tag{17}$$

where V is the volume of the given cubic phase. When the experimental scattering pattern has been fitted with modeled intensities for a given layer width L, the intensity of the 000 reflection can be extracted from the relation

$$I_{000} = I_{000}^{(\mathrm{mod})}(L)\,\frac{I_{hkl}^{(\mathrm{exp})}}{I_{hkl}^{(\mathrm{mod})}(L)} \tag{18}$$

thus the volume ratio of the D and P phase is

$$\frac{V^{(\mathrm{D})}}{V^{(\mathrm{P})}} = \left(\frac{I_{000}^{(\mathrm{D})}}{I_{000}^{(\mathrm{P})}}\right)^{1/2}\left(\frac{\phi^{(\mathrm{P})}}{\phi^{(\mathrm{D})}}\right) \tag{19}$$

Substituting the values of $\phi^{(\mathrm{D})} = \phi^{(\mathrm{P})} = 0.15$, $I_{110}^{(\mathrm{D,exp})} = 84$ (arbitrary units), $I_{110}^{(\mathrm{P,exp})} = 17$ (arbitrary units), $I_{110}^{(\mathrm{D,mod})}(L(\phi{=}0.15)) = 2.638$, $I_{110}^{(\mathrm{P,mod})}(L(\phi{=}0.15)) = 2.364$, $I_{000}^{(\mathrm{D,mod})} = 3.690$, and $I_{000}^{(\mathrm{P,mod})} = 5.502$ we obtain

$$V^{(\mathrm{D})}/V^{(\mathrm{P})} \approx 1.7 \tag{20}$$

a value that would be very difficult to determine without the analysis of the peak intensities. Furthermore having this kind of data for a whole range of the temperature scan, one could determine the phase transition speed, which together with information on the third metastable phase could lead to a better understanding of the phase transition mechanisms.

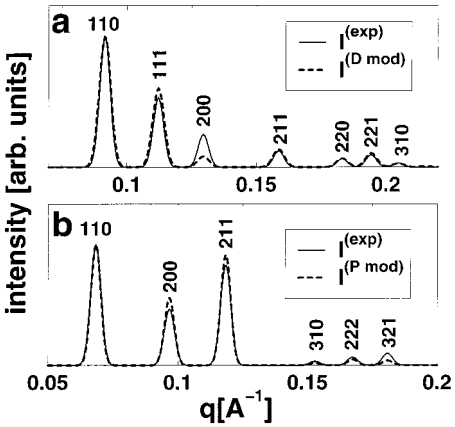

Figure 5. The scattering patterns reported in ref 8 (solid lines) together with the theoretical fits (dashed lines): (a) a D-based phase ($\phi = 0.45$); (b) a P-based phase ($\phi = 0.5$). See section 3.2.1.

3.2. The GMO Systems. The GMO/Polaxmer 407/Water System. 3.2.1. The GMO/Polaxamer 407/Water System.[8] In ref 8, a study of a glycerolmonooleate (GMO) with an addition of a $PEO_{98}PPO_{67}PEO_{98}$ (Polaxamer 407) polymer mixture in excess water is presented. We have been able to extract data of two scattering patterns: one for a 4 wt % polymer to GMO ratio (Figure 5a) and the second for a 7.4 wt % ratio (Figure 5b). The first system has been successfully fitted with a D-based structure of the layer volume fraction $\phi = 0.45$. A too small value of the 200 fitted intensity in comparison to the measured one could be explained by a small addition of the hexagonal phase which in fact has been reported in this system.[8] The superposition of the 10 peak originating from the hexagonal phase on the 200 Bragg reflection of the double-diamond D-based phase is yet another confirmation of the epitaxial relationship described above for the DLPE[4] and DOPE[5] systems. The areas per surfactant head for $\phi = 0.45$ are $a_{s,dir} = 39$ Å^2 for a direct phase and $a_{s,inv} = 48$ Å^2 for an inverse structure. The value of 39 Å^2 seems more resonable, and thus we propose a D direct phase for this system.

The second scattering pattern has been fitted with the intensities of the P-based structure: $\phi = 0.5$, $a_{s,dir} = a_{s,inv} = 36.7$ Å^2. In this case we cannot distinguish the direct from the inverse structures.

3.2.2. The GMO/Polaxamer 407/Water System.[9] As in the last example, the system under investigation is the GMO/Polaxamer 407/water mixture. Reference 9 presents a thorough examination of its phase behavior. Besides the hexagonal and lamellar structures, Landh shows[9]

(7) Li, X.; Kunieda, H. *Langmuir* **2000**, *16*, 10092−10100.

(8) Gustafsson, J.; Ljusberg-Wahren, H.; Almgren, M.; Larsson, K. *Langmuir* **1997**, *13*, 6964−6971.

(9) Landh, T. *J. Phys. Chem.* **1994**, *98*, 8453−8467.

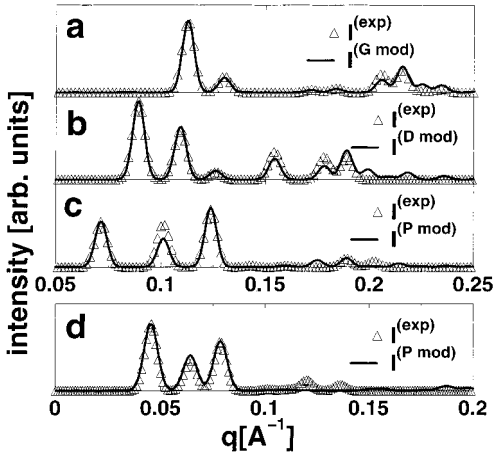

Figure 6. Successful fits of four scattering patterns reported in ref 9: (a) a G gyroid cubic phase; (b) a D double diamond cubic phase; (c and d) two P-based cubic phases. The experimental patterns are drawn with open triangles and theoretical fits with solid lines.

several scattering patterns from the cubic phase region in the phase diagram.

Four of the experimental patterns together with our fits are shown in Figure 6. In the case of all of the presented patterns, the modeled intensities fitted the experimental scattering curves quite well. The data for all these fits are included in Table 1. To enhance the analysis of the structure type, we made an attempt to compare the fitted volume fraction ϕ of the layer decorating the TPMS with the joined volume fraction $\phi_{GMO+P407}$ of surfactant and polymer in the system. For the mixture of composition ($c_{GMO}/c_{P407}/c_{water}$) wt %, we have

$$\phi_{GMO+P407} = \frac{\frac{x_{GMO}}{\rho_{GMO}} + \frac{x_{P407}}{\rho_{P407}}}{\frac{x_{GMO}}{\rho_{GMO}} + \frac{x_{P407}}{\rho_{P407}} + \frac{x_{water}}{\rho_{water}}} \qquad (21)$$

where $x_i = c_i/100$ are the weight fractions.

For the first three systems, both the fitted volume fractions ϕ of the layer compared with the joined volume fraction $\phi_{GMO+P407}$ of surfactant and polymer and the surface areas per surfactant head point out to the direct structures. The data are convincing enough to risk a statement that ascribing these patterns to inverse phases in ref 9 was wrong. In the case of the fourth system, it is impossible to decide which type of the P structure has formed. The fitted volume fraction ϕ suggests an inverse phase, but the area per surfactant head is more resonable for the direct structure. As was noted in ref 9, on increase of the water weight fraction, the system underwent a phase transition. Thus a transition from a direct to an inverse phase could be possible. For even higher water weight fraction ($c_{water} > 50$), L and h have recorded a diffraction pattern, interpreted as evidence of the appearance of the C(P) based cubic phase. A typical pattern from this region (34.18/14.77/51.05) is shown in Figure 7a. In ref 9 it was suggested that the $1{:}\sqrt{2}{:}\sqrt{3}{:}\sqrt{4}{:}\sqrt{5}{:}\sqrt{7}{:}\sqrt{8}$ reflections originate from a C(P) structure with a lattice parameter $a = 315.3$ Å. However we could not fit the experimental pattern with the C(P) spectrum for any layer width ϕ. To illustrate how different the C(P) patterns are, we have showed the $I^{(C(P)mod)}$ (eq 10 for $\phi = 0.3$, 0.5, and 0.7 (Figure 7b−d). Thus we suggest that it is not a C(P)-based phase but rather a P-based phase coexisting with some unknown phase.

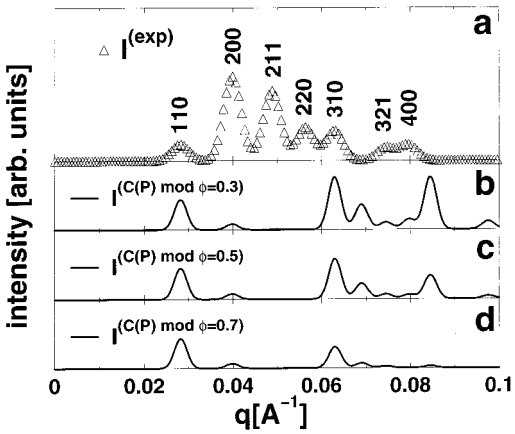

Figure 7. Experimental scatttering curve from ref 9 shown with open triangles (a). Its ascription to a C(P)-based phase was wrong as seen from comparison with three theoretical patterns for this structure for $\phi = 0.3$, $\phi = 0.5$, and $\phi = 0.7$ (b, c, and d, respectively).

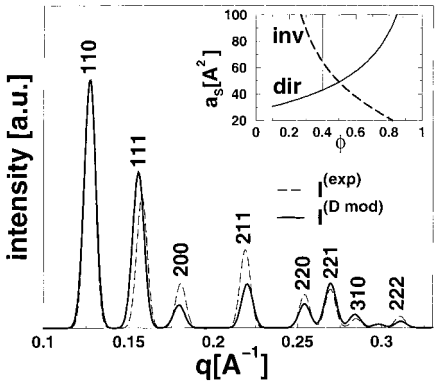

Figure 8. A fit for a DDAB/cyclohexane/water system described in ref 10. The experimental intensity is shown with a dashed line while solid line presents a theoretical pattern for a D TPMS based cubic phase with the layer volume fraction $\phi = 0.4$. Although the fit is not perfect, the value of the area per surfactant head for an inverse phase ($a_{s,inv}(\phi = 0.4) = 64.6$ Å^2 confirms the choice of the structure and layer width. The areas per DDAB per molecule for a direct (solid line) and inverse (dashed line) structures are shown in the inset.

3.3. The DDAB/Cyclohexane/Water System.[10] The system was composed of didodecyldimethylammonium bromide (DDAB), cyclohexane, and water. We have been able to extract the scattering intensity from two scattering patterns. The first one was of a composition (52.9/13.2/33.9) wt % of DDAB/C_6H_{12}/H_2O. The experimental scattering pattern together with the model fit for a double-diamond D-based phase is shown in Figure 8. The best fit was obtained for $\phi = 0.4$. For this ϕ value the areas per surfactant head (for $\rho_{DDAB} = 1$ (g/cm^3), $\rho_{C_6H_{12}} = 0.78$ (g/cm^3), and $a = 120$ Å) are $a_{s,dir} = 43$ Å^2 for a direct phase and $a_{s,inv} = 64.6$ Å^2 for an inverse one. The second value is similar to that proposed by Barois $a_s = 68$ Å^2.[10] It is also in good agreement with an expected chain length of the DDAB molecule. The molecular weight of DDAB is $M_{DDAB} = 462$ (g/cm^3), thus for $a_s \approx 65$ Å^2, it's length is $l_s = V_{DDAB}/a_s = M_{DDAB}/(0.6023\rho_{DDAB}) \approx 12$ Å. Furthermore for the lattice parameter $a = 120$ Å and for the layers volume fraction $\phi = 0.4$, the corresponding layer width $L = 0.22a = 26.4$ Å. Thus the layer width is approximately twice as large as the length of the surfactant molecule ($L \approx 2l_s$). All this evidence stands in favor of an inverse structure.

(10) Barois, P.; Eidam, D.; Hyde, S. T. *Colloq. Phys. J. Phys.* **1990**, *C7*, 25−34.

Table 1. The Data for GMO/P407/Water System Reported in Ref 9[a]

composition (wt %) ($c_{GMO}/c_{P407}/c_{water}$)	fitted TPMS	a (Å)	fitted ϕ	$\phi_{ch} = 1 - \phi$	$\phi_{GMO+P407}$ eq 21	a_s (Å) DIR	a_s (Å) INV	prop. type	prop. type (ref 9)
(68.62/1.99/29.39)	G	136.6	0.25	0.75	0.718	38	114	DIR	INV
(63.1/1.0/35.9)	D	99.7	0.3	0.7	0.654	34	79.3	DIR	INV
(60.08/5.12/34.8)	P	124.3	0.4	0.6	0.664	39	58.4	DIR	INV
(38.66/14.09/47.25)	P	195.6	0.55	0.45	0.538	37.3	30.5	?	INV

[a] The first column gives the weight fractions of the explored mixtures. The second column shows the type of the structure, for which we have fitted the theoretical scattering pattern to the experimental data. The fits are presented graphically in Figure 6. The following columns contain the lattice parameter a, the volume fraction of the layer (ϕ) for which the best fit was obtained, and the volume fraction of the two disjoint channels ($\phi_{ch} = 1 - \phi$). These two values should be compared with the joined volume fractions of the surfactant and polymer (sixth column). In the first three cases the $\phi_{GMO+P407}$ values are similar to the volume fractions of the channels which indicate a direct type of the cubic phase. Small differences (up to ~10%) may be caused by the fact that due to a flat density profile approximation (see ref 1) we determine the width of the layer of an effective contrast which might be slightly different than the actual layer width including the surfactant heads. Another possible explanation is the fact that the phase is polycrystalline with regions of microemulsion, sponge phase, or even excess water. Thus the composition of the system might not reflect the composition of the cubic phase exactly. The seventh and eight columns present the computed surface areas per surfactant head for a direct and inverse structures for the layer volume fraction given in column four. The last two columns show our determination of the structure type compared with the one presented in ref 9. In the case of the first three systems, both the volume fractions and areas per surfactant head point to the direct phases. For the fourth system, the volume fraction suggests an inverse type while the area per surfactant head is more resonable for the direct phase. Since the differences for a direct and inverse phases are quite small, we cease to determine the structure type.

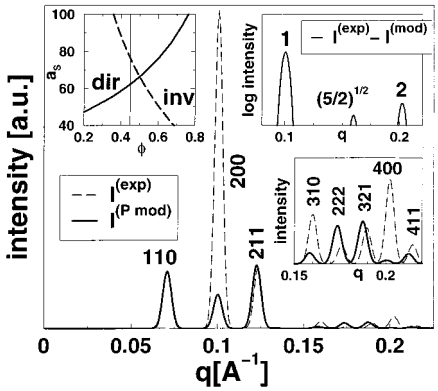

Figure 9. The experimental scattering intensity reported in ref 10 is shown with a dashed line in the main figure and the lower right inset. The best fit with theoretical spectra was obtained for a P-based structure for $\phi = 0.45$ (solid line). The 110, 211, 222, 321, and 411 reflections are reconstructed quite well. The areas per surfactant head for a direct (solid line) and inverse type (dashed line) of the P structure are drawn in the top left inset. The top right one shows the difference between the experimental intensity and the fitted pattern for a P structure. The remaining peaks spaced at the ratio 1:2 are characteristic of a lamellar phase indicating a phase coexistence. The $\sqrt{5/2}$ peak might originate at some transition state.

The second scattering pattern has been recorded for a mixture of composition (41.7/9.3/49) wt % of DDAB/C_6H_{12}/H_2O, respectively. The experimental scattering curve is shown in Figure 9. The authors of ref 10 suggested that this pattern originates from a P-based structure. Indeed, we obtained the best fit for the *P* structure with $\phi = 0.45$. The 110, 211, and 321 peaks are reconstructed very accurately. The 222 and 411 reflections have acceptable values. Furthermore the area per surfactant for a direct phase $a_{s,dir} = 62.3$ Å^2 confirms the choice of a P direct structure. However the intensities of the 200 and 400 experimental peaks are by far greater than the modeled ones. After subtraction of the modeled intensities from the experimental pattern, we have obtained a pattern typical for a lamellar structure (see inset in the right top corner of Figure 10). From the peak positions, one can deduce the lamellar repeat distance d to cubic lattice parameter a ratio: $d/a = 1/2$. Thus we conclude that the investigated mixture was in fact a two-phase region. Furthermore the epitaxial relationship between the lattice parameters of the cubic and lamellar phase suggests a phase transition mechanism illustrated in Figure 10.

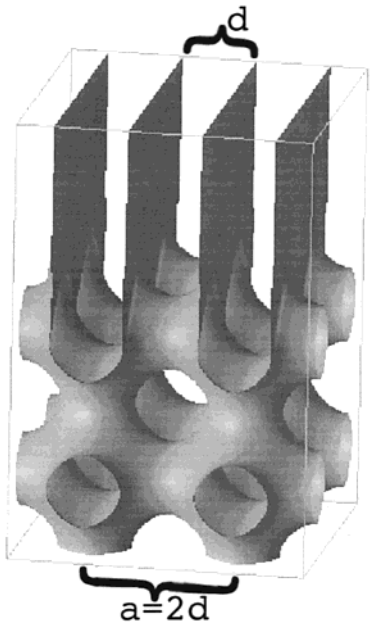

Figure 10. Schematic illustration of the lamellar to P TPMS based cubic phase transition and coexistence. The ratio between the cubic lattice constant a and the lamellar repeat distance d is indicated by the X-ray spectra (ref 10).

Namely, when the phase boundary is crossed from the lamellar region to the P region, the number of passages drastically increases. At some point the passages order in the 2D lamellar planes in a square lattice to form a P-based cubic structure.

3.4. Polymerized G Structure.[11] The system described in ref 11 was an aqueous solution of a cetyltrimethylammonium chloride (CTAC) with an addition of tetraethyl orthosilicate (TEOS). After reaching equilibrium, the system was left for several hours in order to let the hydrolysis of TEOS take place. Next the mesoporous solids obtained in the polimerization reaction were analyzed. Figure 11 shows the experimental scattering pattern of the mesoporous material of the $Ia\bar{3}d$ symmetry. This spectrum was successfully fitted with the scattering intensities for a G-based structure of the layer volume fraction $\phi = 0.45$. The corresponding layer width is $L = 0.149a = 14.6$ Å. Thus fitting the scattering pattern can

(11) Lee, Y. S.; Surjadi, D.; Rathman, J. F. *Langmuir* **2000**, *16*, 195−202.

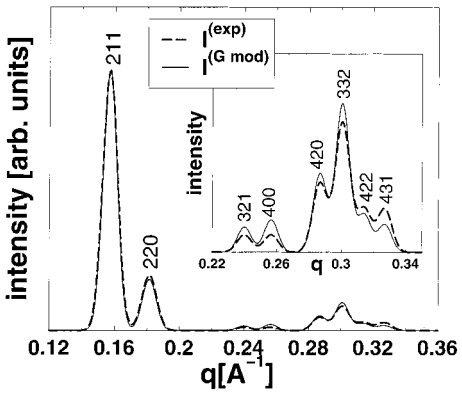

Figure 11. Comparison of the experimental (ref 11) scattering pattern of a polimerized mesoporous material of an $Ia\bar{3}d$ symmetry (dashed line) with a theoretical spectrum for a gyroid G TPMS based phase of a layer volume fraction $\phi = 0.45$ (solid line).

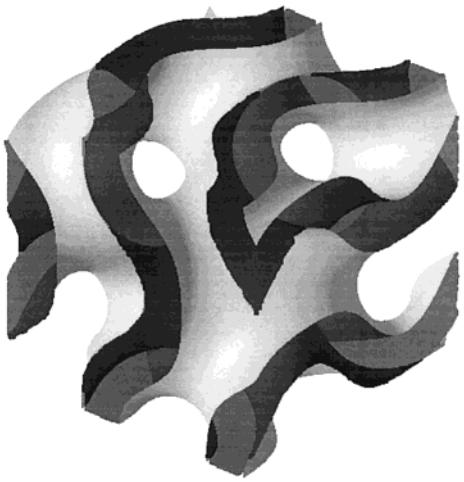

Figure 12. A computer visualization of the G gyroid TPS based cubic phase determined by fitting the experimental SAXS pattern (Figure 11). The darker areas correspond to the subvolume ($\phi = 0.45$) occupied by the polimerized bilayer. See section 3.4 for explanation.

also be a method for an efficient layer width measurement. The visualization of this mesoporous structure is presented in Figure 12.

3.5. The $R_6^F\Sigma EO_2$/Water System.[12] This last example is meant to show that the analysis of the intensity of the Bragg reflections can be done without performing the fitting procedure given by eq 11. This method is particularly useful when the intensities of several reflections are very small. In the preliminary analysis, it is enough to draw the relative intensity of the strongest reflections with respect to one reference peak as a function of the layer width L

$$I_{hkl}(L)[I_{HKL}] = \frac{I_{hkl}{}^{(\mathrm{mod})}(L)}{I_{HKL}{}^{(\mathrm{mod})}(L)} \qquad (22)$$

The reference peak should have a large intensity and possibly the smallest HKL indices. In the case of all three simple structures P, D, and G, the first reflection is a good candidate. Figure 13 shows the intensities of the strongest

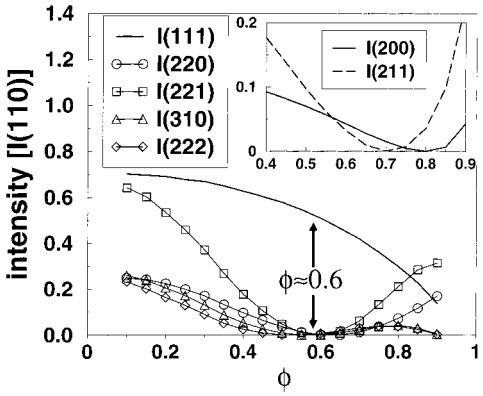

Figure 13. The theoretical intensities for the D TPMS based phase of the 111 (solid line), 220 (circles), 221 (squares), 310 (triangles), and 222 (diamonds) reflections expressed in terms of the intensity of the 110 peak. The arrows mark the layer volume fraction $\phi \approx 0.6$ for which the theoretical intensities are in accordance with experimental measurements.[12] The 111 intensity has been measured to be $I_{111} \approx 0.5I_{110}$ while the 220, 221, 310, and 222 peaks were very weak ($<0.01I_{110}$). The inset shows the theoretical intensities of the 200 and 211 reflection, experimentally measured to be $I_{200} \approx 0.01$ and $I_{211} \approx 0.03$.

Table 2. The Experimental Intensities Reported in Ref[12]

spacing	*hkl* assignment	$I^{(\mathrm{exp})}$
$\sqrt{2}$	110	1
$\sqrt{3}$	111	~0.5
$\sqrt{4}$	200	~0.01
$\sqrt{6}$	211	~0.03
$\sqrt{8}$	220	< 0.01
$\sqrt{9}$	221	< 0.01
$\sqrt{10}$	310	0
$\sqrt{12}$	222	0

[a] The first column contains the spacing of the observed peaks, the second the *hkl* assignment, and the last column contains the intensities expressed in terms of the intensity of the first (110) reflection.

reflections of the D-based phase in terms of the reference peak $HKL = 110$. These in turn can be compared with analogously expressed intensities of the experimental scattering pattern of the fluorinated surfactant $C_6F_{13}C_2H_4$-$SC_2H_4(OC_2H_4)_2OH$ ($R_6^F\Sigma EO_2$)/water system reported in ref 12. The experimental intensities are presented in Table 2. The intensity of 111 peak $I_{111}{}^{(\mathrm{exp})} \sim 0.5$, the small values of the 200, 211, 220, and 221 reflections, and absence of the 310 and 222 reflections are in good agreement with the theoretical values for the layer volume fraction $\phi \approx 0.6$. Furthermore at this value of ϕ, the 200 and 211 reflections are significantly greater than zero, which is in accordance with the experimental measurement. It is important to note here that the intensity of the 200 reflection might be in fact bigger than the intensity of the 211 peak as expected by the theory. Due to rather small resolution of the scattering patterns presented in ref 12, the 200 peak lays within the vicinity of the broad 111 reflection. Thus its intensity is probably underestimated.

4. Conclusions

We have presented a simple method for a quantitative analysis of the scattering patterns of self-assembled cubic phases in amphiphilic mixtures. Many examples presented in this paper prove the utility of the method. In a few cases it provided very interesting insight into the structure and thermodynamic stability of aqueous dispersions of

(12) Ropers, M. H.; Stebe, M. J.; Schmitt, V. *J. Phys. Chem. B* **1999**, *103*, 3468−3475.

various surface active agents. We propose this method as an ordinary practice in exploring the cubic regions of binary and ternary mixtures. We believe that together with the presently applied methods, it will deepen our knowledge of these fascinating systems. Especially in time-resolved techniques when the scattering patterns are recorded for different temperatures, a detailed analysis of the spectra should yield important information concerning the transition rates, phase coexistence, structural changes, elasticity constants, etc.

Acknowledgment. This work has been supported by the KBN Grant 5 P03B 094 21 (2001−2003) and 5 P03B 084 21 (2000−2001).

LA011299H